Oxygen-related defect characterization using correlative microscopy

Amanda Youssef[1], Erin E. Looney[1], Mallory A. Jensen[1], Ashley E. Morishige[1], Sebastian Mack[2], Sarah Wieghold[1], Hannu S. Laine[3], Jeremy R. Poindexter[1], Barry Lai[4], Hele Savin[3], Tonio Buonassisi[1]

[1] Massachusetts Institute of Technology, Cambridge, Massachusetts, 02139, USA
[2] Fraunhofer Institute for Solar Energy Systems, Heidenhofstraβe 2, D-79110 Freiburg, Germany
[3] Aalto University, 02150 Espoo, Finland
[3] Advanced Photon Source, Argonne National Laboratory, Argonne, IL 60439, USA

***Abstract* — Swirl defects caused by oxide-related defects, namely oxide precipitates, have a detrimental effect on solar cell performance as these defects act as sinks for metal impurities. We suggest a method that allows the characterization of oxygen-related defects, which are suspected to be on the scale of a few tens of nanometers, which, despite their small size, have a macroscale effect on the minority carrier lifetime. The method consists of a suite of microscopy technique applied together to a) locate the defects and map them in a statistically relevant area, b) measure their density, size and distribution within the wafer bulk, and c) study their morphology and chemical state. As a result, we can understand the root-cause behind the formation of the oxide-related defects, their gettering ability, so we can apply processing techniques to mitigate them.**

I. Introduction

Swirl defects revealed as concentric rings of low lifetime [1], cause a conversion efficiency drop of 20% relative [2] as observed previously [3]–[5]. Additionally, 30% of the ingot is severely affected by swirl defects, which decreases manufacturing yield. By understanding the root-cause behind swirl defects, we can effectively mitigate them by applying tailored engineering techniques. By doing so, we improve both the device performance and the manufacturing yield, which reduces the capital expenditure and hence the cost of solar energy [6], [7].

Oxygen in monocrystalline silicon is introduced into the silicon melt from the silica crucible and gets incorporated into the Czochralski crystal during growth [1]. Point defects are formed during the process, affected by growth parameters such as the temperature gradient and the ingot pulling rate, and act as oxygen nucleation sites. Under high temperature processes during the solar cell fabrication, oxygen nuclei grow to become strained precipitates. Excess silicon atoms are kicked out as the precipitate grows to form crystallographic defects. Strained oxide precipitates and their associated crystallographic defects such as stacking faults and dislocation loops act as internal gettering sites for metal impurities [7]. Since the oxygen content in an ingot is a function of the ingot height, the impact of the swirl defect is also a function of the ingot position: areas with higher oxygen content lead to larger and higher density oxide precipitates, which result in stronger swirl defects.

In this work, we suggest a correlative microscopy approach to characterize in three dimensions the distribution of oxide-related defects, their density, size [8] and morphology and their gettering effect inside swirl defect areas. The main challenge, is that oxide-related defects causing low lifetime concentric circles on the macroscale are in fact nanometer scale defects in monocrystalline silicon, which makes them hard to localize. For this reason, we mark the defects by intentionally contaminating samples with known bulk micro-defect (BMD) density. We then apply a set of microscopy techniques: synchrotron-based micro x-ray fluorescence (μ-XRF), micro x-ray absorption near edge spectroscopy (μ-XANES), electron beam induced current (EBIC), and transmission electron microscopy (TEM). We then apply the same correlative techniques to wafers exhibiting swirl defects and compare the results. μ-XANES gives information about the chemical state of the copper precipitates. μ-XRF shows the density of the decorated BMDs as a function of copper drive-in temperature, while EBIC tomography gives information about the distribution of these defects within the bulk in three dimensions as well as their recombination activity. TEM, on the other hand, demonstrates morphology and chemical state as well as metal decoration of the precipitates.

II. Methods

A. Sample Preparation

Three double-side polished *p*-type silicon samples with doping level of $9x10^{14}$ cm^{-3}, (100) crystal orientation and bulk micro-defect density between 2.4×10^{10} and 3.2×10^{10} cm^{-3} are laser cut to 1x1 cm^2 samples and etched to remove about 5 μm from the surface before subjecting them to an RCA clean. We dip the samples in a copper chloride solution with a concentration of 0.5 mol/L, prepared using copper (II) chloride dihydrate ($CuCl_2$, $2H_2O$) from Sigma Aldrich. Each sample is then annealed in a tube furnace at a different temperature, namely 700°C, 900°C and 1000°C, for 30s. These parameters are enough for the copper to diffuse through the whole thickness of these wafers. All samples undergo similar air cooling while being extracted from the tube at an estimated rate of 25°C/s. Finally the samples are etched using CP4 to remove any remaining copper on the surface.

An *n*-type sample exhibiting swirl defects, and a sample in which intentional oxide precipitates were grown following the method developed by Falster *et al.* [9], have been cleaned, contaminated and etched similarly to the way described above.

For EBIC measurements, diodes have been prepared from the same samples measured with µ-XRF. For *p*-type silicon, samples are etched in hot nitric acid at 80°C for about 10 min to grow a chemical oxide. Then, a 50 nm thick aluminum layer is thermally evaporated. For *n*-type silicon, samples are dipped in hydrofluoric acid to remove the native oxide, then a 50 nm thick layer of gold is deposited using e-beam evaporation.

B. Measurement Techniques

Synchrotron-based µ-XRF and micro x-ray absorption near edge spectroscopy (µ-XANES) are performed using an incident X-ray beam with energies of 10 keV, for the samples with known BMD density shown in figure 2, and 9 keV for the samples with intentionally grown oxygen precipitates and swirl defects shown in figure 5. For µ-XRF, a step size of 220 nm and a dwell time of 100 ms per spot is used to map 50×50 μm^2 or smaller areas using the flyscan mode [10]. For µ-XANES measurements of Cu, CuO, Cu_2O, Cu_3Si, and Cu_5Si standards are acquired for comparison (plotted in the results are only CuO, Cu_2O, and Cu_3Si, for clarity). The measurements are carried out at Argonne National Laboratory's Advanced Photon Source Beamline 2-ID-D.

EBIC tomography is performed using a Hitachi dual focused ion beam / scanning electron microscope system. The varied accelerating voltage determines the variation in the penetration depth of the exciting electron beam and hence allows mapping the defects in three dimensions, which is not possible using µ-XRF alone.

III. RESULTS

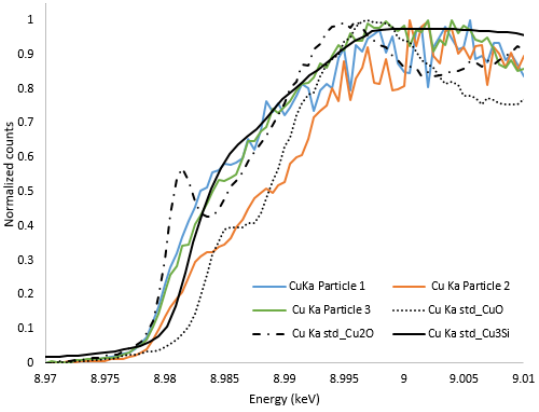

Fig. 1. µ-XANES spectra of CuO, Cu_3Si, and Cu_2O standards, along with three different precipitates, randomly selected, from the sample with copper drive-in temperature of 1000°C. Two precipitates show a trend following Cu_3Si, one appears close to follow more CuO.

Figure 1 shows µ-XANES spectra for the Cu contaminated samples at 1000C and standards to identify the charge state of the copper precipitate. Three precipitates are analyzed. Cu_3Si appears to be the most energetically favorable form of copper in silicon as previously shown [11], [12]. However one of the measured precipitates shows a different behavior and might be associated with a copper oxide chemical state. We hypothesize that this particle formed at the surface either by out-diffusion or by decorating a defect close to the surface. It is to be noted that consequently, in our precipitate size calculations we have adopted a copper precipitate with a Cu_3Si phase. EBIC measurements would reveal the depth distribution of these copper decorated bulk-microdefects to provide the full picture.

Figure 2 shows the copper channel of a µ-XRF map collected from 50x50 μm^2 on each of the three *p*-type samples that are subjected to high temperature copper diffusion temperatures of 1000°C, 900°C, and 700°C respectively. Our results show that the contamination method is well-controlled, since only copper is detected whereas all other transition metals that could have potentially been incorporated show counts below noise level. At a 1000°C drive-in temperature, we detect 165 precipitates with a platelet shape. Given the information depth of Cu-Kα XRF emission of 12.77 um, we measure a volumetric density of approximately 5.2×10^9 cm^{-3}. At a drive-in temperature of 900°C, we detect 395 precipitates with a measured volumetric density of 1.2×10^{10} cm^{-3}; however, the particles exhibit a mix between platelet and point-like features. Lastly, at a drive-in temperature of 700°C, we detect 700 precipitates in the probed volume all represented as point-like features, and giving a volumetric density of 2.2×10^{10} cm^{-3}.

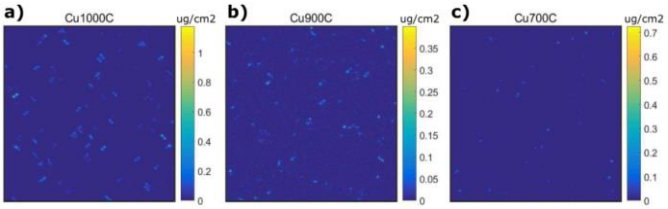

Fig. 2. Quantified copper channel of 50×50 μm^2, 0.22 µm step size, 100 ms dwell time in flyscan mode µ-XRF for *p*-type silicon samples contaminated with copper at different drive-in temperatures a) 1000°C, b) 900°C and c) 700°C.

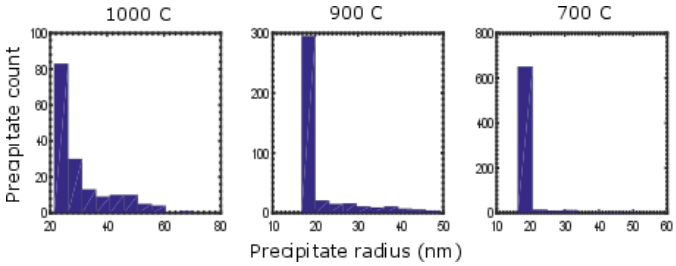

Fig. 3. Histograms of precipitate radii distribution for *p*-type silicon wafers contaminated with copper at 1000°C, 900°C and 700°C respectively.

Figure 2 is not enough since the smaller precipitates cannot be easily seen in the map, but are detected by the computer program. Copper precipitate radii are plotted in the histograms shown in figure 3. We observe a spread in the precipitate radii for the sample subjected to a drive-in temperature at 1000°C with most of the particles being as small at 25nm in radius. As we drive the copper at lower temperature, the detected precipitates are more homogeneous in size with radius around 20 nm.

As an investigation of whether the high temperature anneals are in fact dissolving oxygen-related defects, all three *p*-type silicon samples that are subjected to high temperature copper diffusion temperatures of 1000°C, 900°C, and 700°C respectively are measured with Fourier transform infrared spectroscopy (FTIR). An additional control sample with the same bulk microdefect density that is not subjected to any high temperature annealing is also measured alongside with the processed samples for comparison. The FTIR data in figure 4, shows no change in the interstitial oxygen peak (1107 cm^{-1}) in all four spectra, proving that the high diffusion temperature is not dissolving the oxygen-related defects in any of the samples in question, and the BMD density is expected to remain between $2.4x10^{10}$ and $3.2x10^{10}$ cm^{-3}.

Further, we apply similar measurements to a set of samples in which one has intentionally grown oxygen precipitates and another exhibits swirl defects. The samples undergo similar intentional copper contamination, but in this case the drive-in temperature is performed at 1000°C only. Figure 5 shows quantified µ-XRF maps of the copper channel for both a) a sample with homogeneously and intentionally grown oxygen precipitates and b) a sample where the region of low lifetime of the swirl defect is scanned. The shape of the copper particles differs from the samples with known BMD density (compare Fig. 1). We hypothesize that this is caused by the fact that the previous samples have bulk micro-defects that are not strictly oxide precipitates and hence copper decoration of these different crystallographic defects behaves differently. In the specific case of the sample shown in figure 5 b), iron was also detected overlapping with the copper particles. We hypothesize that since this sample was processed similarly to a solar cell, some of the iron was internally gettered to the oxide precipitates at the swirl defect region, instead of being gettered out by the phosphorus diffusion gettering step.

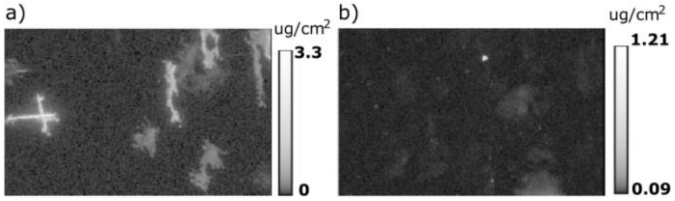

Fig. 5. Quantified µ-XRF maps showing the copper channel for a) a 50x40 um^2 area of a silicon wafer subjected to similar processing that would create the magic denuded zone, developed by Falster et al., which grows uniformly oxide precipitates in the bulk and b) a 50x30 um^2 area of low lifetime swirl defect from a *n*-type PV-grade silicon wafer.

IV. Conclusions

In this contribution, we develop a technique to characterize oxygen-related defects within a statistically relevant area. We intentionally contaminate with copper silicon samples with a known bulk micro-defect density, a sample with known oxide precipitate density and a sample exhibiting swirl defects. We then perform a suite of microscopy techniques, namely µ-XRF and EBIC to measure density, three-dimensional distribution, size and chemical state of copper decoration at these bulk micro-defects. EBIC measurements as well as TEM will be included in the complete study.

References

[1] A. Borghesi, B. Pivac, A. Sassella, and A. Stella, "Oxygen precipitation in silicon," *J. Appl. Phys.*, vol. 77, no. 9, pp. 4169–4244, May 1995.

[2] J. Haunschild, I. E. Reis, J. Geilker, and S. Rein, "Detecting efficiency-limiting defects in Czochralski-grown silicon wafers in solar cell production using photoluminescence imaging," *Phys. Status Solidi RRL - Rapid Res. Lett.*, vol. 5, no. 5–6, pp. 199–201, Jun. 2011.

[3] M. Kivambe *et al.*, "Minority-carrier lifetime and defect content of n-type silicon grown by the noncontact crucible method," *J. Cryst. Growth*, vol. 407, pp. 31–36, Dec. 2014.

[4] C. Jun-ichi and S. Shozo, "Swirl defects in silicon crystals," in *Proceedings of the 10th conference on Solid State Devices*, Tokyo, 1979, vol. 18, pp. 153–164.

[5] A. Youssef *et al.*, "Swirl defect investigation using temperature- and injection-dependent photoluminescence imaging," presented at the 43rd IEEE PVSC, Portland, OR, 2016.

[6] D. B. Needleman, J. R. Poindexter, R. C. Kurchin, I. Marius Peters, G. Wilson, and T. Buonassisi, "Economically sustainable scaling of photovoltaics to meet climate targets," *Energy Env. Sci*, vol. 9, no. 6, pp. 2122–2129, 2016.

[7] W. von Ammon, "FZ and CZ crystal growth: Cost driving factors and new perspectives: FZ and CZ crystal growth," *Phys. Status Solidi A*, vol. 211, no. 11, pp. 2461–2470, Nov. 2014.

[8] D. P. Fenning *et al.*, "Precipitated iron: A limit on gettering efficacy in multicrystalline silicon," *J. Appl. Phys.*, vol. 113, no. 4, p. 44521, 2013.

[9] R. Falster, M. Cornara, D. Gambaro, M. Olmo, and M. Pagani, "Effect of High Temperature Pre-Anneal on Oxygen Precipitates Nucleation Kinetics in Si," *Solid State Phenom.*, vol. 57–58, pp. 123–128, 1997.

[10] A. E. Morishige *et al.*, "Accelerating synchrotron-based materials characterization: leveraging flyscan capability," *(Submitted)*.

[11] T. Buonassisi *et al.*, "Synchrotron-based investigations of the nature and impact of iron contamination in multicrystalline silicon solar cells," *J. Appl. Phys.*, vol. 97, no. 7, p. 74901, 2005.

[12] A. A. Istratov, T. Buonassisi, M. A. Marcus, T. F. Ciszek, and E. R. Weber, "Dependence of precipitation behavior of Cu and Ni in CZ and multicrystalline silicon on cooling conditions," in *Proceedings of the 14th NREL Workshop on Crystalline Silicon Solar Cell Materials and Processes, Winter Park, USA*, 2004, pp. 165–169.